Environmental Fluid Mechanics
https://doi.org/10.1007/s10652-022-09861-6

ORIGINAL ARTICLE

Investigation of flow structure with moat acting as a water cushion at the toe of an overflowing levee

Fakhar Muhammad Abbas[1] · **Norio Tanaka**[1,2]

Received: 18 March 2021 / Accepted: 1 April 2022

Abstract

The principle theme of this study is to introduce a novel countermeasure to reduce the energy of the overflowing floodwater by utilization of a water cushion. For this purpose, laboratory experiments including "LW" cases (levee with water cushion) and "OL" cases (only levee) were conducted to elucidate the role of a water cushion in the flow structure variation after a levee is overflowed and to reduce energy. A moat (a deep and wide trench) with varying non-dimensional length ($L_m{*}=L_m/h_L$; L_m is the length of the moat where h_L is the levee height) and depth ($D_m{*}=D_m/h_L$; D_m is the moat depth) acting as a water cushion was provided at the toe of a levee with varied landward slopes (S_L). The energy reductions in the LW and OL systems were found to be very close to each other at lower overflow water depths, while it was 25% greater in the LW system than in the OL system at higher overflow water depths. Changes in the landward slope (S_L) of the levee, non-dimensional length ($L_m{*}$), and depth ($D_m{*}$) of moat significantly changed the flow structure and created six different flow structures. However, 1–6%, 1–3%, and 1–5% differences in energy reduction rate were observed by varying S_L, $L_m{*}$, and $D_m{*}$, respectively, in LW cases. All flow structures contributed greatly to energy reduction, but the energy reduction rate was maximum in flow structure named as T-2. Flow structures named as T-2 and T-6 are preferable due to increased water depth inside the moat and presence of submerged hydraulic jump which can be achieved during landward slopes S_L = 1:1, 1:2 and by decreasing $L_m{*}$ $D_m{*}$, of moat during Landward slope S_L = 1:3.

Article Highlights

- The water cushion function of moat was utilized at toe of overflowing levee.
- The effect of different non-dimensional overflow water depths, non-dimensional length, depth of moat and varying landward slope of levee on flow structure was investigated.
- Different flow structure was classified based on non-dimensional length and depth of moat.
- Relation between flow structure and energy reduction rate was investigated.

✉ Norio Tanaka
tanaka01@mail.saitama-u.ac.jp

[1] Graduate School of Science and Engineering, Saitama University, 255 Shimo-okubo, Sakura-ku, Saitama-shi, Saitama 338-8570, Japan

[2] International Institute for Resilient Society, Saitama University, Saitama, Japan

Keywords Overflowing levee · Moat · Energy reduction · Classification of flow structure

1 Introduction

Floods are natural disasters that cause massive destruction to property, crops, and loss of human lives. Although many countries attempted to eliminate and minimize flood damage by constructing dams, reservoirs, levees, and retarding basins. The existing mega-flood control measures are constructed to handle major flood events that usually occur once every 150–200 years. Among these structures, levees are important for flow channelization to protect people and riverine areas from flood inundation because more than 80% of past flood disasters have been ascribed to overflowing levees [1]. Once overflow from a levee has occurred, it applies an intense erosive force on the toe of the levee due to high energy, which finally causes the failure of the levee [2]. In recent years, flooding has occurred more frequently in Japan due to global climate change and severe weather conditions [3].

The 2011 Great East Japan Tsunami (GEJT) caused large scale flooding that caused huge devastation of defence structures, including tsunami gates, sea walls, embankments [4], and coastal forests [5]. The Ministry of Land, Infrastructure, Transport, and Tourism of Japan (MLIT) classified it as a level 2 tsunami with an expected return period of hundreds to a 1000 years [6]. The inundation depth of a level 2 tsunami exceeded the capacity of defence structures and embankments were overflowed [7]. To mitigate the hinterland damage by overflowing water, a compound defence strategy consisting of a combination of natural and artificial structures was proposed. Many studies and much effort have been deployed to devise a compound defence system including coastal vegetation and an embankment [8–10], a moat (a deep and wide trench) and a forest [11], a canal and a dune [12, 13], a moat behind an embankment [14, 15], double embankments [16], a forest embankment and a moat [17], and a multiple line defence strategy [18, 19].

During the GEJT, coastal vegetation planted downstream of a dike played an important role in mitigating the energy of overflowing water by the formation of a hydraulic jump [20]. However, although vegetation in front of an embankment proved beneficial for reducing flow energy and overflow volume [8], there was a risk of erosion, which can uproot the vegetation [6]. The direct collision of flow with vegetation or a forest can seriously damage it, as was observed during the GEJT [5]. A compound defence system containing an intentionally constructed forest/vegetation area requires much space on the landward side, and growing tall trees densely is difficult [21, 22]. A hydraulic jump formed, or resistance offered by a second embankment behind the first overflowing embankment could increase the energy reduction, but there is a risk that the second embankment will be washed out when the second embankment is made of soil [7]. To reduce the risk of washing out the second embankment, Igarashi et al. [7] further proposed a line of vertical piles behind the embankment, although this idea was advantageous for reduction of the energy, it was not economical to build rows of lined piles. The protective measures were applied on the toe of the levee to mitigate the energy, including concrete blocks [23], geogrid [24], riprap, coreloc and utilization of the underlayer with riprap and coreloc [25]. Although these measures protect the toe of the levee, the scour hole was shifted further downstream, which would be dangerous for downstream structures [26]. It is also very difficult to install protective measures up to a vast-areas on downstream, which will be of no further use.

During the 2004 Indian Ocean tsunami, the Buckingham Canal played a significant role in mitigating tsunami damages [27] and Tanaka et al. [28] pointed out that ditches and pools of water were generated as scour phenomena behind overflowing embankments during the GEJT, and the accumulated water in these ditches acted play an important role in scour prevention. Similarly, a moat along with a forest and an embankment greatly reduced the fluid force and overflow volume [17, 29]. Li et al. [30] proposed a water cushion to protect the bottom of a stilling basin and dissipate the energy and pointed out that it buffered the main flow and played a key role in minimizing the bottom velocity. The function of a water cushion as a countermeasure against the damage caused by overflowing and breaching of a levee has still not been studied comprehensively. Based on previous studies, it is very important to investigate the complete dynamics and utilization of a water cushion as a countermeasure to reduce the energy of overflowing flood flows.

Therefore, the main objective of this study was to develop and formulate a novel countermeasure to diminish flood damage by reducing the flood energy due to overflowing flood water. For this purpose, a water cushion (also known as a "flexible bottom plate" [31]) was installed in the toe region of the levee by providing a moat structure. This water cushion structure was expected to not only provide a counterforce to overflowing water but also absorb the impact of the flow, as described by [30].

2 Materials and methods

2.1 Flow conditions

Laboratory experiments were performed in a rectangular open channel having a length, width, and depth of 14 m, 0.5 m, and 0.7 m, respectively, at Saitama University, Japan. The laboratory flume and experimental setup is presented in Fig. 1a, b. During laboratory experiments, the ground conditions (i.e., ground topography, slope etc.) were not specific to any location but were considered generally as adopted by [26]. In the 2011 Great East Japan Tsunami (GEJT), the overtopping depths ranged from 0.84 to 1.78 m and were recorded around the Abukumagawa river embankment located in the Tohoku region of Japan [28]. During the post tsunami surveys conducted by Tokida and Tanimoto [32], the overtopping depths were observed to be between 2.8 and 6.8 m. Usually, a large flood flow occur with a long period in inland areas, and its regeneration in an experimental scenario is very difficult and not suitable for adequate scaling, whereas the flood flow in the flume could be generated by a control pump discharge (m^3/s) [33]. Moreover, flood waves are often referred to as quasi-steady flows because of their long duration [16]. Thus, steady state can be adopted to model large flood flows.The pump discharge (m^3/s) was used to generate the flood wave in this investigation to ensure proper scaling on a 1/100 scale. Previously [6, 7, 17, 21, 26, 29, 34] have utilized the steady flow conditions with model scale experiments (1/100) in laboratory flume to replicate the real scenario. On the other hand, there is chance of surface tension distortion occurrence in the flow structure if we consider the non-steady case. Moreover, Froude similarity is adopted to replicate the real scenario of flood flow in free surface gravity flows considering the small-scale experiments. Therefore, taking previous literature as a reference, the present study considered the model scale 1/100 with steady flow conditions to represent the actual scenario. Furthermore, in support to the above statement, Igarashi and Tanaka [7] conducted both small (1/100) and large (1/50) scale physical

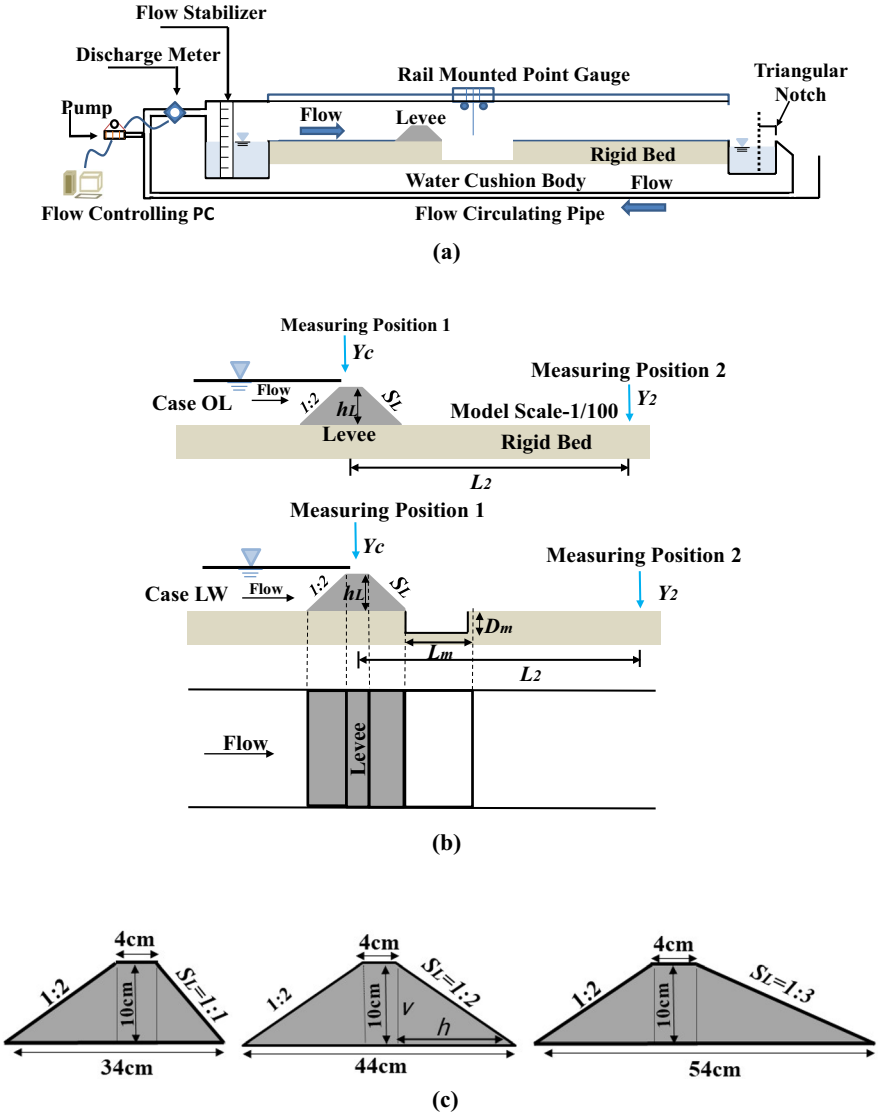

Fig. 1 Experimental setup **a** Laboratory Flume **b** Setup of levee and moat model. (Note: OL represents levee only; "LW" represents levee with water cushion body), **c** Levee model with varying landward slope

experiments in order to determine the energy loss behind the region of embankment and lined piles. They stated that, the flow behavior has the similar trend and is unaffected by energy loss mechanism by changing the scale of the model although the effect of large scale difference was not elucidated. Thus, considering the actual case, a model scale of 1/100 and five quasi-steady overflow flow depth conditions ranging between ($Yc = 1.8–4$) cm were set for all the experimental trails to replicate a real scale flood flow as already adopted by [7, 16]. The range of overflow water depth was adopted

between the minimum and maximum overflow depth that was recorded in the above mentioned studies. To obtain the desired critical overflowing flow depths, Froude similarity was used. The Froude number was calculated in an empty channel without placing any modal because due to reflection of water by the embankment, the flow shifted to subciritical at the upstream side of the embankment. Therefore, the flow conditions were thus achieved in an empty channel to ensure, mimic, and replicate the real overflowing depths. Before settling on the range of flow conditions to be evaluated, a number of discharge trials were carried out. Water depths were determined using a rail-mounted point gauge against each discharge number, and used to estimate the Froude number and critical water depth. As a result, five initial Froude numbers i.e., ranged from $\left(Fr_1 = 1 - 1.2\right)$, were obtained from the five initial water depths $\left(Y_c = 1.8 - 4\ \text{cm}\right)$ and discharge values. Once the appropriate flow conditions were achieved, which replicated the original overflowing flow characteristics, the embankment model with various configurations of moat was then put into the experimental flume for further testing.

2.2 Model characteristics

The experimental setup consisted of a levee and a water cushion body (moat). A moat, with the assumption that it could reduce the energy of overflowing flood water by forming a hydraulic jump or counterforce within a moat. The levee and moat were also replicated in this research, similar to the modeling of overtopping water depths, for improved replication of the modeled structures. Following the Great East Japan Earthquake of 2011, the Japanese government intended to raise and/or rebuild the coastal embankments in Fukushima, Miyagi, and Iwate prefectures to a height of (7.25–14.7 m) to reduce the impact of a level 2 tsunami [18, 34]. Therefore, in this study, on a 1/100 scale, the levee was scaled down to 10 cm in height, with a constant river slope of 1:2, while varying landward slope (S_L = 1:1, 1:2, 1:3) as shown in Fig. 1c. The moat was attached directly at the toe of the levee model (provided at 4 m from upstream of channel) without any gap. Although some authors [17, 29, 35] have already utilized the trapezoidal moat, the supercritical high energy flow is accelerated on the downstream landward slope of the embankment and the slope of the moat which directly hits the ground of the trapezoidal moat, which was not suitable. Hence, a moat with a rectangular shape was utilized in the present study to investigate its effectiveness in flood energy mitigation. It was assumed that the high energy super critical flow directly interacts with the accumulated water of the rectangular moat instead of the ground surface, and that the front vertical face of the rectangular moat can further reduce the energy by flow reflection. In terms of effectiveness, the basic role of defense structure depends mainly on the reduction of damage downstream of it by decreasing the specific energy of flow. Therefore, this study focuses solely on the flow structure variation and energy reduction rate by considering a fixed moat with varying lengths and depths which is similar to previous studies [17, 29, 35, 36]. Previously, Ahmed et al. [35] utilized a 40 cm long moat in laboratory experiments, while Tokida and Tanimoto [9] reported a 26.3 m-long moat (dug pool) during a field survey. To keep things consistent with previous studies, the length of moat (L_m) was selected as 25, 30 and 35 cm respectively. The wooden material was used to design the levee and moat structures. In total, 30 cases and 150 experimental trials were conducted as described in Table 1.

Table 1 Experimental conditions

No.	Case name	(S_L)	L_m*(=L_m/h_L)	D_m*(=D_m/h_L)	Y_c*(=Y_c/h_L)
1	$OL_{1:1}$	1:1	–	–	0.18, 0.24, 0.29, 0.35, 0.4
2	$OL_{1:2}$	1:2	–	–	0.18, 0.24, 0.29, 0.35, 0.4
3	$OL_{1:3}$	1:3	–	–	0.18, 0.24, 0.29, 0.35, 0.4
4	$LW_{A\text{-}B\text{-}C}$	1:1, 1:2, 1:3	2.5, 3.0, 3.5	0.5, 0.7, 1	0.18, 0.24, 0.29, 0.35, 0.4

LW represents the levee with a water cushion body, *OL* represents a levee only. In $LW_{A\text{-}B\text{-}C,}$ A expresses the landward slope (S_L); B expresses the non-dimensional length of the water cushion body (L_m*); C represent the non-dimensional depth of the moat (D_m*)

2.3 Water depth and velocity measurement

The water depth was measured along the centerline of the channel and at predetermined measuring positions 1 and 2 as shown in Fig. 1b by a point gauge (Tokyo Keisoku Company Ltd., Tokyo, Japan, HAT-106, HAT-30) with an accuracy of (± 0.0001 m) which was mounted on the rail. The water level fluctuations were observed at measuring position 2 during formation of the hydraulic jump so that the average, maximum, and minimum values were taken. The flow surface inside the moat was complex, so the water depth was measured by two different methods (direct point guage and video analysis for flow visualization) at every 1 cm interval to observe the flow surface variation inside the maot. The maximum and minimum depths were averaged after being measured numerous times at a fixed location with surface variation. While the water level was measured at every 5 cm interval behind the moat. In order to take video of the flow for counter checking of the measured water profiles by point guage, a PC running photography software (K-II Ver.1.03) operated a high-speed digital camera (Kato-koen Company, Ltd.). Outside the glass side wall of the flume, a transparent scale was connected to record this footage. Finally, a software (Flow expert Ver.1.2.6 by (Kato-koen Co Limited)) was used to analyze the video and identify the water level. The continuity equation ($Q = V_1 Ycb = V_2 Y_2 b$, where Q is the discharge in m^3/s, b is the channel width, Yc and Y_2 are water depths at measuring positions 1 and 2), which was utilized to estimate the depth-averaged velocities, V_1 and V_2, at measuring positions 1 and 2, respectively.

2.4 Method for evaluating flood energy reduction rate

During all cases of "OL" and "LW", measuring position 1 at the crest of the levee (to measure overflowing water depth Y_c) and measuring position 2 at a certain distance (L_2) behind the levee (where flow tended to become almost uniform) were fixed as water level measuring positions, as shown in Fig. 1b.The energy reduction rate ΔE[%] was calculated to estimate the effectiveness of the moat by the formula:

$$\Delta E[\%] = \frac{E_1 - E_2}{E_1} \times 100 \tag{1}$$

where E_1 is the energy head (sum of the potential head (Y_c) and velocity head ($V_1^2/2\,g$; V_1 is depth-averaged velocity; g is gravitational acceleration) at measuring Position 1, and E_2

is the energy head (sum of the potential head (Y_2) and velocity head ($V_2^2/2\,g$; V_2 is depth-averaged velocity) at measuring position 2.

2.5 Non-dimensional parameters

To observe and investigate the actual phenomena in laboratory experiments, it is necessary to scale down the physical model of the original prototype to a smaller size and contemplate some similarity to the original prototype, including force, motion, or geometry. So that the results obtained from laboratory experiments can be utilized for prediction of prototype behavior. Utilizing important hydraulic and physical model parameters used in this study as shown in Fig. 1, the following dimensional group was formed.

$$f_1\left(\Delta E, Y_C, L_m, D_m, h_L, h, V, V_C, V_2, Y_2, E_1, E_2, g, \rho, \mu, \sigma\right) = 0$$

$\Delta E = E_1 - E_2$ is the energy reduction rate, Y_C is critical flow depth at Measuring Position 1, L_m is length of moat, D_m is depth of moat, h_L is height of levee, h and v is the horizontal and vertical side of landward slope of embankment, V_C is velocity at Measuring Position 1, V_2 is velocity at Measuring Position 2, Y_2 is flow depth at Measuring Position 2, E_1 is specific energy at Measuring Position 1, E_2 is specific energy at Measuring Position 2, g is gravitational acceleration, ρ is density of water, μ is viscosity of water, and σ is the surface tension of water.

According to the Buckingham's pi theorem, the dimensionless parameters are summarized as:

$$f\left(\frac{\Delta E}{E_1}, \frac{L_m}{h_L}, \frac{D_m}{h_L}, \frac{Y_C}{h_L}, Fr_1, S_L, R_e, W_e\right) = 0$$

In free surface gravity flow, fluid characteristics such as density and dynamic viscosity of water and air–water surface tension are important factors to take into consideration. Therefore, in order to verify the applicability of this model scale experiment, it is necessary to maintain the same parameters as the actual scale, such as Froude number, Reynolds number, and Weber number. Usually, Froude similarity is used for free surface gravity flows rather than the Reynolds number [6, 21]. In the present study, Froude similarity was used to define the hydraulic conditions (as discussed earlier in Sect. 2.1). Since the density and viscosity of the water were same in every case therefore, the Reynolds number was ignored. In addition, the experiment was conducted in a smooth glass sided wall channel with a very small bed slope, and the water level was measured along the centerline of the channel. Hence, the effect of wall roughness was also eliminated. Furthermore, to minimize the effect of the surface tension of water, which is associated with the non-dimensional weber number, the minimum value of weber number required should be greater than 11 [37]. The weber number for this research varied from 67 to 267. Previously, Peter and waburton [38] also found that the threshold range of Weber number ranged from approximately 10 to 120, and values less than this would result in some surface tension-induced distortion in the modelled experiment. Consequently, the weber number determined in this investigation was larger than 10, So it was assumed that the impact of surface tension on this experiment was thought to be negligible.

This study mainly focused on the energy reduction of a tsunami overtopping flow through the defense system (downstream of the moat model) and therefore the energy reduction rate is a function of dimensionless overtopping depth $\left(Y_C^* = {}^{Y_C}/_{h_L}\right)$, in which Y_C

is estimated from the Froude Similarity (discussed in above Sect. 2.1)), depth $\left(D_m^* = {}^{D_m}/_{h_L}\right)$ and length $\left(L_m^* = {}^{L_m}/_{h_L}\right)$ of moat and slope of the embankment $\left(S_L = h/v\right)$.

$$\frac{\Delta E}{E_1} = f\left(\frac{L_m}{h_L}, \frac{D_m}{h_L}, \frac{Y_C}{h_L}, S_L\right)$$

Three different non-dimensional lengths (L_m*=2.5, 3.0, 3.5) and non-dimensional depths (D_m*=0.5, 0.7, 1) were selected which were not considered according to any specific locations. Three experimental cases with only a levee were conducted for comparison purpose and named as $OL_{1:1}$, $OL_{1:2}$, and $OL_{1:3;}$ where 1:1, 1:2, and 1:3 express the values of S_L For the levee with a moat, the cases were denoted ($LW_{A\text{-}B\text{-}C}$), where A, B, and C express S_L (=1:1, 1:2, or 1:3), Lm* (=2.5, 3.0, or 3.5), and D_m* (=0.5, 0.7, or 1), respectively.

3 Results

3.1 Water profiles and flow structure identification

The flow regime was varied by changing the hydraulic parameters including Y_c*, L_m*, and D_m* of the moat. During only levee "OL" cases, the water depth downstream of the levee decreased on the landward slope, tended to reach a minimum value, and then became uniform at a certain distance behind the levee, as shown in Fig. 2.

Figures 3, 4 and 5 represents the water profiles for all cases during S_L 1:3,1:2 and 1:1, respectively. The x-axis represents the distance along the channel length, whereas the y-axis shows the water depth. It is evident from the schematic diagram of the observed flow structure (Fig. 2) and water profiles (Figs. 3, 4 and 5) that the flow regime varied greatly in the "LW" cases. A high-resolution camera was utilized to visualize the flow structure. After analysis of all experimental trials, Six different flow structures named as, T-1, T-2, T-3, T-4, T-5, and T-6, along with varying hydraulic jumps were identified, as shown in Fig. 2. The generation of these various flow structures and hydraulic jumps was due to the water cushion function of the moat, which provided a counterforce to the mainstream and absorbed the impact of the overflowing flood flow [39].

Flow structure T-1 appeared at lower overflow water depths; an undulating wave with clockwise rollers was generated by the counterforce of the accumulated water inside the moat. At some distance downstream of the moat, the flow became uniform. T-1 was converted into T-2 when a jet flow was generated inside the moat by the increased overflow water depth, which directly hit the face and bed of the moat. The flow emerged into two zones. One bounced upstream and joined the main flow, and the second zone reflected to generate the strong anticlockwise reverse rollers, which tended to generate a completely submerged hydraulic jump starting from the slope of the levee and covering the entire moat (T-2 in Figs. 2, 3, 4, 5). The T-2 flow regimes were interesting compared to T-1 because an undular hydraulic jump was generated behind the moat due to the direct strike an upstream bounced flow joining the mainstream.

During flow structure T-3, wider vortices, and undulating waves (like in T-1) were generated, and an undulating hydraulic jump was generated behind the maot at some distance. There was no hydraulic jump during flow structure T-4, the mainstream flowed over a deep moat without creating any undulating wave. It directly hit the front face of the moat with the generation of medium-sized clockwise vortices and

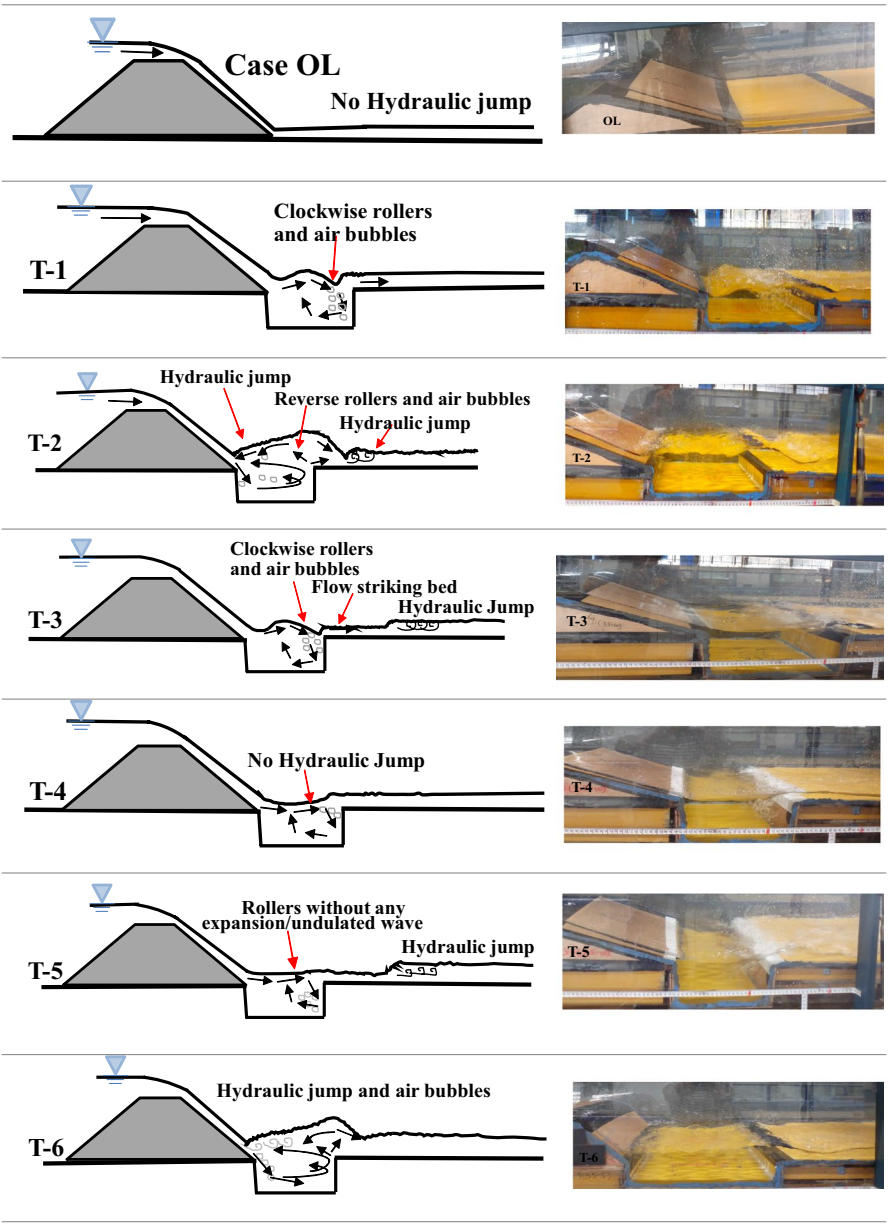

Fig. 2 Classification of flow structures observed

air bubbles near the end of the moat. There was no undulating wave generated inside the moat in T-5. The flow structures T-3 and T-5 were similar to each other because the supercritical flow was generated behind the moat up to a certain distance, and an undular hydraulic jump was formed behind the moat, as shown in Figs. 2, 3, 4 and 5. The flow structure of T-6 was similar to that of T-2: a submerged hydraulic jump

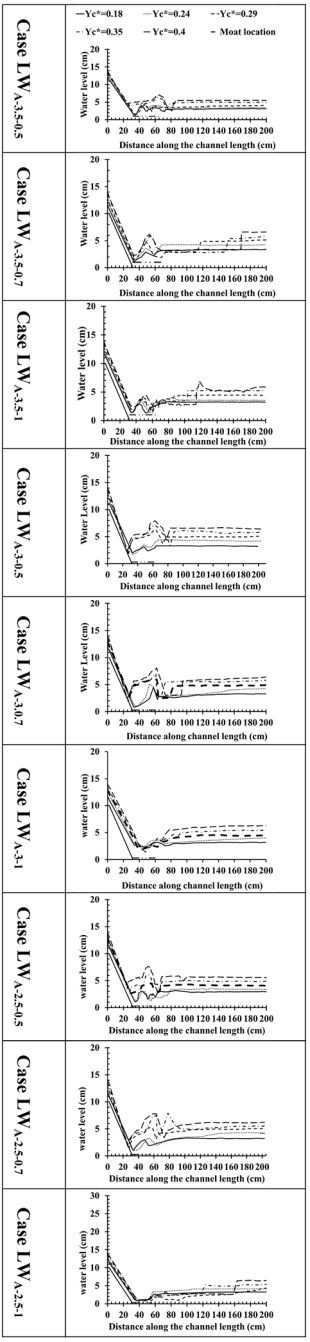

Fig. 3 The longitudinal water profiles during landward slope 1:3

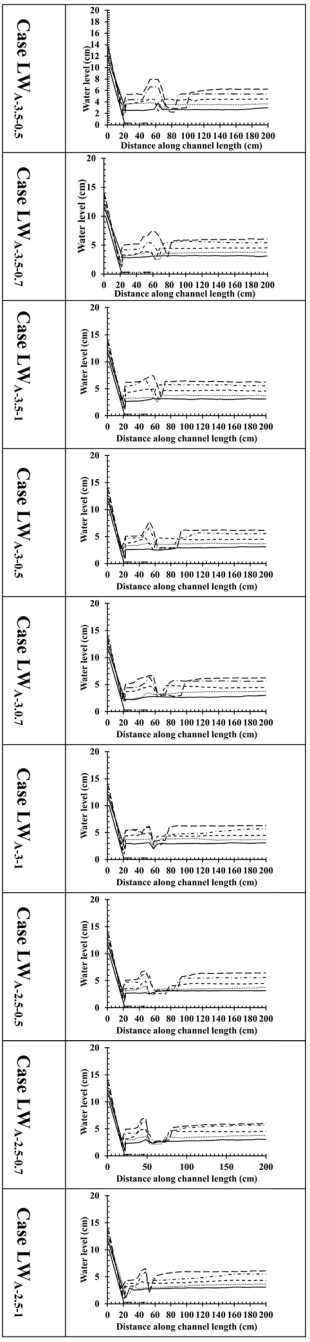

Fig. 4 The longitudinal water profiles during landward slope 1:2

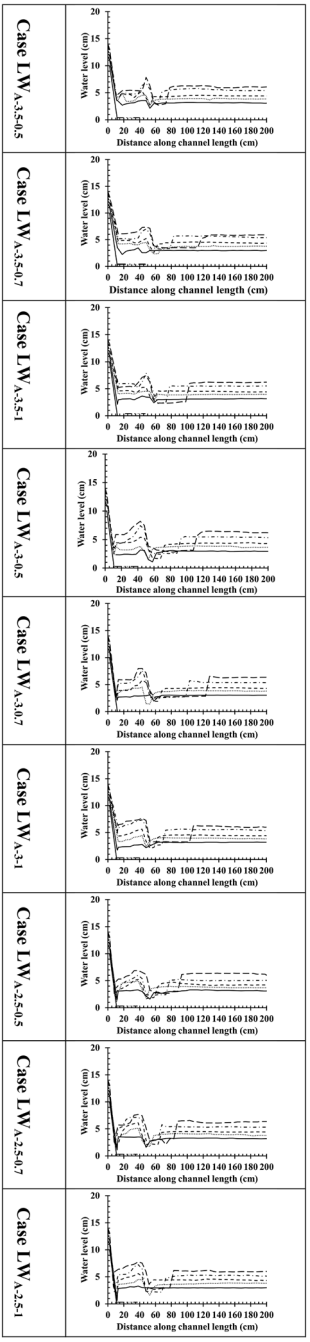

Fig. 5 The longitudinal water profiles during landward slope 1:1

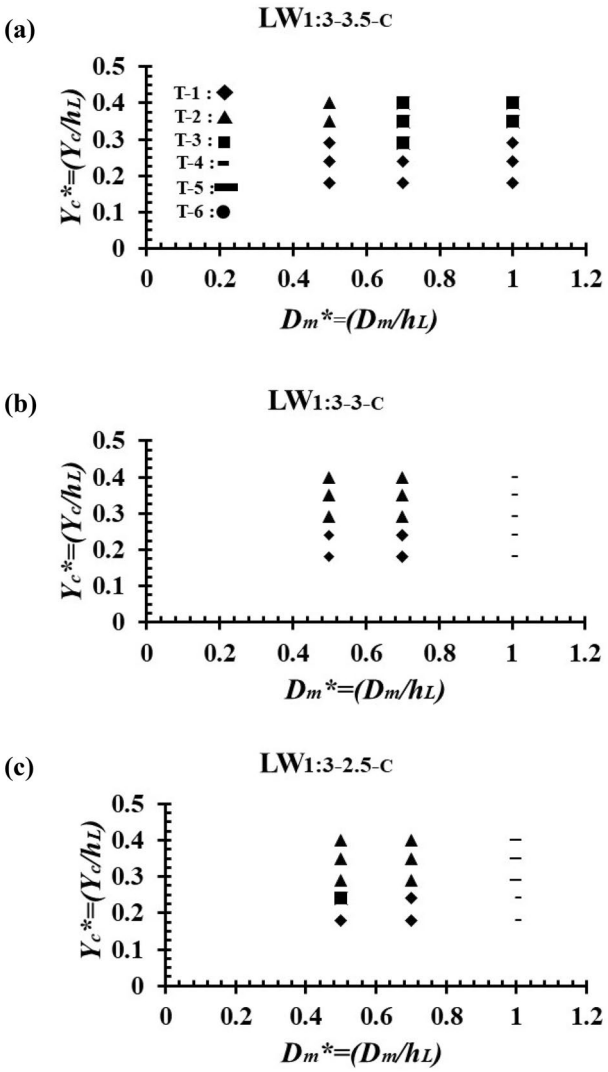

Fig. 6 Flow structure classification with respect to D_m* and L_m* during Landward slope 1:3; **a** Case $LW_{1:3-3.5-C;}$ **b** Case $LW_{1:3-3-C}$ **c** Case $LW_{1:3-2.5-C}$

starting from the slope of the levee was generated and covered the whole moat, but there was no second hydraulic jump behind the moat in T-6. Similar flow structures were also discussed by [6] and it can be concluded from present results that the sufficient increase in water depth inside the moat during flow structures T-2 and T-6, may be proved to be beneficial for energy mitigation.

3.2 Effect of non-dimensional overflow depth (Y_c*), moat length (L_m*) and depth (D_m*) on flow structure classification

Figures 6, 7 and 8 represent the flow structure classification on landward slopes (S_L) 1:3, 1:2, and 1:1, respectively, at various non-dimensional length (L_m*) and depth (D_m*). The

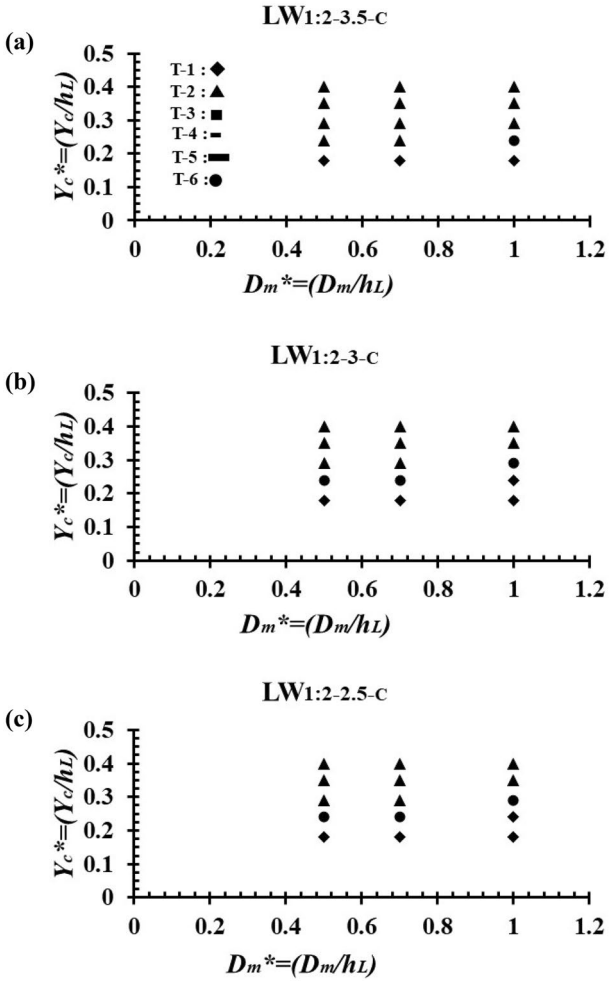

Fig. 7 Flow structure classification with respect to D_m* and L_m* during Landward slope 1:2 **a** Case $LW_{1:2\text{-}3.5\text{-}C;}$ **b** Case $LW_{1:2\text{-}3\text{-}C}$ **c** Case $LW_{1:2\text{-}2.5\text{-}C}$

vertical axis depicts the non-dimensional overtopping depth (Y_c*). As it can be seen in all cases presented in Fig. 6a–c, a variety of flow structures were observed during the landward slope 1:3 because it was a gentle slope compared to slopes 1:1 and 1:2. After overflow from the levee, the water flowed on a long, gentle slope with less gravitational acceleration [40] and lower impact force [41]. When this flow interacted with the water storage of the moat, it generated five varied flow structures, as shown in Fig. 6a–c, depending upon the dimensions of the moat and overflow water flow depths. Figure 6a (case $LW_{1:3\text{-}3.5\text{-}C}$ at D_m*=0.5) shows that the flow structure was related to T-1 at lower overflow water depths (Y_c*=0.18, 0.24, 0.29). While at maximum overflow water depths (Y_c*=0.35, 0.4), the flow structure changed to T-2 due to the generation of strong reverse rollers and backwater reflection by a jet flow that directly hit the bed and front face of the moat. By increasing the non-dimensional depth (D_m*) of the moat from 0.5 to 0.7 and 1 in the case of $LW_{1:3\text{-}3.5\text{-}C}$ (Fig. 6a), the flow regime at lower overflow depths was almost T-1, which was discussed already, but the flow structure turned into T-3 at higher overflow depths. Due to the increasing depth of the moat, the counterforce offered by the moat was increased,

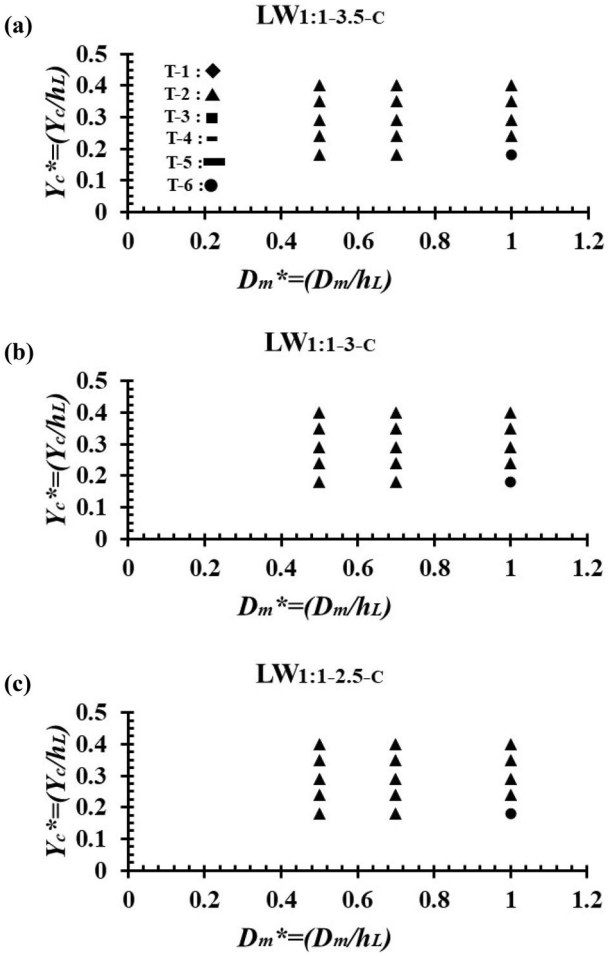

Fig. 8 Flow structure classification with respect to D_m* and L_m* during Landward slope 1:1 **a** Case $LW_{1:1\text{-}3.5\text{-}C;}$ **b** Case $LW_{1:1\text{-}3\text{-}C}$ **c** Case $LW_{1:1\text{-}2.5\text{-}C}$

and did not let the mainstream hit the bed of the moat. As a result, an undulating wave was generated which covered the whole moat, directly struck the bed behind the moat, and generated an undular hydraulic jump, which was already discussed in 3.1. In case $LW_{1:3\text{-}3\text{-}C}$ (Fig. 6b), case $LW_{1:3\text{-}2.5\text{-}C}$ (Fig. 6c), at D_m*=0.5–0.7, the length of the moat was reduced to L_m*=3 and L_m*=2.5, respectively. By changing the parameters of the moat, the flow regime was also varied compared to the previous case $LW_{1:3\text{-}3.5\text{-}C}$ (Fig. 6a). The flow structure became T-2 at the overflow depth (Y_c*=0.29,0.35,0.4). This was different from the previous case $LW_{1:3\text{-}3.5\text{-}C}$ (Fig. 6a) at D_m*=0.5 in which T-2 was observed at only higher overflow depths (Y_c*=0.35 and 0.4). The appearance of T-2 in cases $LW_{1:3\text{-}3\text{-}C}$ (Fig. 6b), $LW_{1:3\text{-}2.5\text{-}C}$ (Fig. 6c), at D_m*=0.5 to 0.7 at a lower overflow depth (Y_c*=0.29) was due to a shorter moat, in which the jet flow hitting the bed and face of the moat was reflected earlier to give rise to T-2 flow dynamics. While the flow structure at lower overflow depths (Y_c*=0.18–0.24) was T-1, in the case of $LW\text{-}_{1:3\text{-}3\text{-}C}$ at D_m*=0.5 and 0.7 (Fig. 6b). However, in case $LW_{1:3\text{-}2.5\text{-}C}$ at D_m*=0.5 (Fig. 6c), T-3 was observed and at (Y_c*=0.24) because of the minimum length (L_m*=2.5) the undulating wave did not remain completely

inside the moat. While the non-dimensional depth of the moat increased from D* = 0.5, 0.7 to D_m* = 1, the flow regime also converted to T-4 in case $LW_{1:3-3-C}$ (Fig. 6b), in which the main stream passed over the deep moat without creating a hydraulic jump. At the same D_m* = 1 in case $LW_{1:3-2.5-C}$ (Fig. 6c), the flow structure observed at higher overflow depths (Y_c* = 0.29, 0.35, 0.4) was T-5 in which a hydraulic jump appeared after some distance behind the moat. From the above description, it can be concluded that with landward slope 1:3 at maximum L_m* = 3.5, the flow structure is shifted from T-1 and T-3 to T-2 and by decreasing L_m* from 3.5 to 3 and 2.5 the flow structure is changed from T-4, T-5, and T-1 to T-2 by decreasing D_m* and increasing Y_c*.

Figure 7a–c represents the flow structure classification during cases with landward slope 1:2. Only three flow structures, T-1,T-2, and T-6, were observed during all cases ($LW_{1:2-B-C}$) of landward slope 1:2. In cases $LW_{1:2-3.5-C}$ at D_m* = 0.5 and 0.7 (Fig. 7a), the flow structure was T-1 at lowest overflow depth (Y_c* = 0.18) while it was converted to T-2 at higher overflow depths (Y_c* = 0.24, 0.29, 0.35, 0.4). Increasing the depth of the moat (D_m* = 1) at the same L_m* = 3.5 caused the flow structure T-6 to appear at Y_c* = 0.24, because the increased counterforce of the deep-water storage by the mainstream cannot push the whole water storage. Thus, flow structure T-2 cannot be obtained,as already discussed. Similarly, during cases $LW_{1:2-3-c}$, $LW_{1:2-2.5-C}$, (Fig. 7b, c), the flow structure was T-2 at higher overflow depths (Y_c* = 0.29, 0.35, 0.4), whereas it was T-1 and T-6 at lower overflow depths (Y_c* = 0.18 and 0.24), respectively, at D_m* = 0.5,0.7. By increasing the depth of the moat D_m* = 1 in cases $LW_{1:2-2.5-C}$ and $LW_{1:2-3-C}$, the flow structure was initially T-1 at Y_c* = 0.18 and 0.24, but it became T-6 at Y_c* = 0.29, and finally was converted to T-2 at highest Y_c* = 0.35 and 0.4, respectively.

Only flow structures T-6 and T-2 were observed during cases $LW_{1:1-B-C}$ (Fig. 8a–c). The flow structure was T-6 at the lowest overflow depth Y_c* = 0.18, and it became T-2 at higher overflow depths Y_c* = 0.24, 0.29, 0.35, and 0.4 in cases $LW_{1:1-3.5-C}$, $LW_{1:1-3-C}$, and $LW_{1:1-2.5-C}$ (Fig. 8), respectively. Hence it can be said that the flow structure was shifted from T-6 to T-2 by increasing Y_c* and decreasing D_m* at the constant landward slope 1:1, as shown in Fig. 8. The main reason for conversion of flow structures to T-2 and T-6 was steep slopes 1:1 and 1:2; on these slopes, the water flowed down faster with the contribution of gravitational acceleration [41] and directly hit the bed of the moat from which it was reflected and generated the T-2 and T-6 respectively. The flow structure T-2 and T-6 can be obtained by decreasing moat length (L_{m*}) and depth (D_{m*}) during landward slope (S_L = 1:3). Whereas, by changing the landward slope (S_L = 1:3–1:2 and 1:1) the flow structure was almost converted into T-2 and T-6.

3.3 Relationship between flow structure and energy reduction rate

The relationship between the energy reduction rate and flow structure classification for the cases of landward slopes 1:3, 1:2, and 1:1 is presented in Figs. 9, 10 and 11, respectively.

In Figs. 9, 10 and 11 it can be observed in all cases that the energy reduction rate in the "LW" cases was relatively larger as compared to the "OL" cases. The energy reduction in the "OL" cases was due to a direct collision of overflowing water with the bed. Energy reduction in the "LW" cases was susceptible to the interaction of the water cushion structure behind the levee, which provided the counterforce and absorbed the impact of overflowing water and generated hydraulic jump [30]. The overall difference of energy reduction rates between LW and OL cases was much less at lower overflow depths (Y_c* = 0.18–0.24). This difference tended to increase with increasing overflow depths and became maximum at the

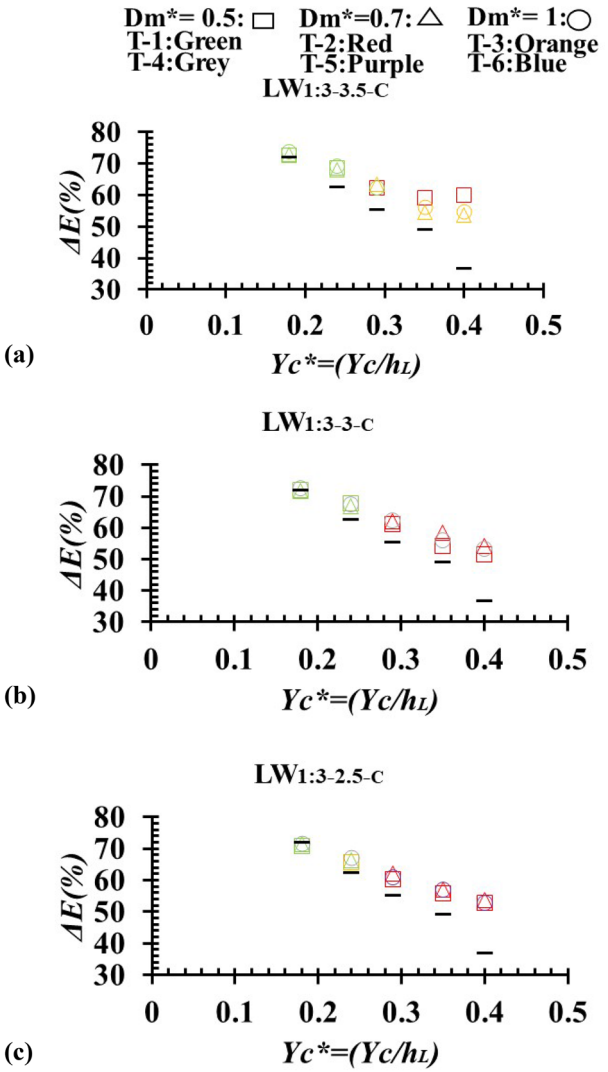

Fig. 9 Energy reduction for cases with landward slope 1:3. **a** Case $LW_{1:3\text{-}3.5\text{-}C.}$ **b** case $LW_{1:3\text{-}3\text{-}C.}$ **c** case $LW_{1:3\text{-}2.5\text{-}C}$

highest overflow depth (Y_c*=0.4) in all cases, as shown in Figs. 9, 10 and 11, respectively. It was noted in all cases that the energy reduction rate in "LW" cases was maximum for the flow structure T-2, where it was approximately 25% higher as compared to the OL system. While the energy reduction rate was 18%, 16%, 17% and 8% higher during flow structures T-3, T-4, T-5, and T-1 as compared to OL cases, respectively. It was also observed that the energy reduction rate was maximum for landward slope 1:1 and minimum for landward slope 1:3 in all cases of OL and LW systems, respectively. The larger energy reductions for landward slopes 1:1 and 1:2 was due to direct collision of accelerated flow (on steep slope due to increased gravitational effect) with the water cushion bed and formation of a T-2 flow structure. On the gentle landward slope 1:3, the flow was not as fast as on the steep slopes [40]. It passed over the moat at lower overflow depths while the T-2 flow structure was also observed during some cases only at higher overflow depths. Hence the overall

energy reduction rate on the gentle S_L 1:3 was smaller than that on steep slopes. It can be concluded that changing the landward slope S_L of the levee and dimensions of the moat non-dimensional depth D_m* and length L_m* varied the flow structure greatly, but the difference in energy reduction among LW cases was not greater. Only 1–3%, 1–5%, and 1–6% differences in energy reduction were caused by changing L_m*, D_m* and S_L, respectively, for all LW cases. The above discussion demonstrates that variations in the landward slope and dimensions of the moat play important roles in changing the flow structure but did not significantly reduce the energy reduction rate.

4 Discussion

4.1 Variation in flow structure

For levee-only cases, the flow becomes supercritical after it overflows the levee and strikes the downstream levee toe at a higher velocity. Due to the high energy of overflowing flood water, the levee failure started from its toe which extended towards the crest [42, 43]. For this reason, many coastal structures, trees, and residential areas were severely damaged during the GEJT [28, 44]. Thus, a secondary structure behind the embankment/levee is needed to reduce the flow velocity. The water depth can be raised within the structure by placing an obstacle downstream of the slope, and a hydraulic jump can be generated [45, 46]. The force and velocity of flow can be decreased by increasing the water depth [20, 47]. Hence, in the present study, a moat was provided in the toe region of the levee as a secondary obstacle, and it acted like a water cushion in "LW" cases. In "LW" cases (levee with moat), six different flow structures were observed depending upon the dimensions of the moat (L_m*, D_m*) and landward slope (S_L) of the levee, which were described in previous section.

Igarashi and Tanaka [16] reported an experimental investigation of the effectiveness of a second embankment behind the first embankment to reduce the energy of the overflow flow. Four different flow structures were observed, Type c was closely related to T-2 in this study. A submerged hydraulic jump starting from the landward slope of levee and covering the whole moat was formed. But the formation of Type c in igarashi's study [16] occurred at lower overflow depths, and when the overflow depth was increased, the flow structure turned into other types and created a risk of washing out the second embankment. In contrast, the T-2 in the current study was generated at higher overflow depths only, as was discussed with detail in previous sections. The effect of lined piles behind the overflowing embankment was investigated by [7], and they observed ten different flow structures, A1–A6 and B1–B4, respectively. In flow structures A1–A5 and B1, the mitigation of the tsunami was maximum. The flow structures T-3 and T-5 of the present study were like the B-1 in which the hydraulic jump appeared behind the moat. while A-6 and T-4 were very similar, having no hydraulic jump and flow remaining supercritical. The hydraulic jump just behind the moat in T-2 was like that in A-3 in which the hydraulic jump formed due to striking free nap flow behind the lined piles. Similarly, the parameters of a previous study including non-dimensional overflow depth, non-dimensional height of piles, number of rows of piles, non-dimensional spacing of lined piles, and parameters of the present study Y_c*, D_m*, and L_m* greatly affected the flow structure variation and formation of a hydraulic jump, but the flow structures B2 and B3 in previous study conducted by Igarashi et al. [7] were not feasible due to generation of a standing wave.

Muhammad and Tanaka [6] also defined A and B-type flow structures in an experimental study comprising an overflowing embankment and vegetation. During the A-type flow, a hydraulic jump was generated on the flume bed between the overflowing embankment and vegetation, while the hydraulic jump was shifted towards the slope of the embankment and covered the entire region of defense structures in the B-type flow, which closely resembled T-2 and T-6 of present study. The hydraulic jump in which its toe is shifted towards the slope of the levee could be proved very beneficial for the safety of structure because it significantly reduces the downstream velocity [45, 47]. Therefore, the formation of a B-type hydraulic jump was more appropriate for sustaining the hydraulic structure, as T-2 and T-6 of the present study showed. Similarly, Kamiwada et al. [29] also utilized the combination of an embankment, moat, and vegetation and found that the arrangement with an embankment, moat, and vegetation was very advantageous to a flow structure with higher water depth and lower flow velocity. The moat in the present study and their study played a key role as a moat to generate the hydraulic jump.

All parameters, including non-dimensional depth D_m*, length L_m* of the moat, non-dimensional overflow depth Y_c*, and S_L effectively affected the flow structure variation. The flow structures T-2 and T-6 were advantageous for the sustainability of the structures due to their higher water depth. Hence, in present study, it was found that these flow structures (T-2 and T-6) was achieved with decreasing *Lm** and *Dm** at higher *Yc** during $S_L = 1{:}3$. Because during lower $Dm^* = 0.5$–0.7 and $Lm^* = 3$, 2.5, the approaching overflowing water directly hits the bed and front face of the moat, which generates the reverse rollers and backwater reflection. Whereas this type of flow phenomena was not generated during highest $Lm^* = 3.5$ and $Dm^* = 1$. On contrarily, the flow structure was almost shifted towards T-2 and T-6 during $S_L = (1{:}2,\ 1{:}1)$ and all overtopping depth. The recommended zone to obtain T-2 and T-6 is given in Fig. 12 for more clarification. The current research did not take into account the different shapes of moats and heights of levees; however, the flow structure and energy reduction rate might be altered by modifying the form of the moats as well as considering different heights of levees. Hence, these results cannot be recommended for all shapes of moats and different heights of levee. Further study is needed to investigate flow structure variation by providing various shapes of moats and levee height.

4.2 Energy reduction

The energy reduction in LW cases was approximately 25% greater than that in OL cases as already discussed in Sect. 3.3 and shown in Figs. 9, 10 and 11 respectively. The energy reduction in the OL system was due to direct collision of overflow water with the downstream flume bed, whereas the energy reduction in the LW system was mainly due to the counterforce offered by the accumulated water (water cushion effect) [31], during the interaction of the mainstream flow with the moat, which also generated a hydraulic jump. A maximum energy reduction of 25% was observed during T-2 and T-6, in which a submerged hydraulic jump starting from the slope of the levee was formed and an undular hydraulic jump was generated due to direct collision with mainstream flow. Igarashi and Tanaka [16] also found similar results and showed that the energy reduction rate was 20% higher in a double embankment system due to formation of a hydraulic jump by free nap flow as compared to a single embankment. The energy reduction rate was 18%, 16%, 17%, and 8% in flow structures T-3, T-4, and T-5, and T-1, respectively. The formation of a hydraulic jump plays a key role for energy reduction in high-speed flood overflow [7, 47]. Muhammad and Tanaka [6], Pasha and Tanaka [21], Ali

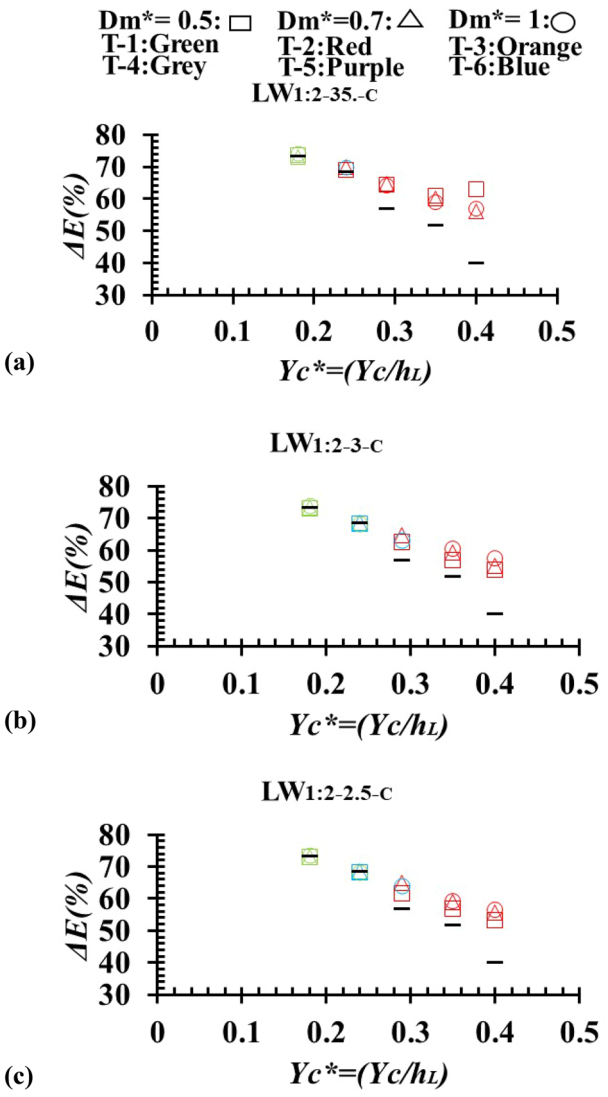

Fig. 10 Energy reduction rate for the cases with landward slope 1:2. **a** Case $LW_{1:2\text{-}3.5\text{-}C}$, **b** case $LW_{1:2\text{-}3\text{-}C}$, **c** case $LW_{1:2\text{-}2.5\text{-}C}$

et al. [48], Rashedunnabi and Tanaka [49] investigated the contribution of a hydraulic jump to energy reduction of the flow by utilizing coastal vegetation of varying densities and found that the dense vegetation reduced the energy more. Igarashi et al. [7], who reported that the energy reduction was increased by increasing pile height, the main reason for formation of a hydraulic jump. In contrast, the present study showed that the energy reduction during LW (levee with water cushion) was 5–25% greater as compared to OL (Only levee) cases. It was mainly due to the presence of the water cushion effect. Overall, six different flow structures were observed during LW (levee with water cushion) cases. The changing parameters L_m*, D_m* of the moat and landward slope of levee (S_L) greatly affected the flow structure variation as well as the energy redction rate. All observed flow structure greatly influenced the energy reduction rate whereas the flow

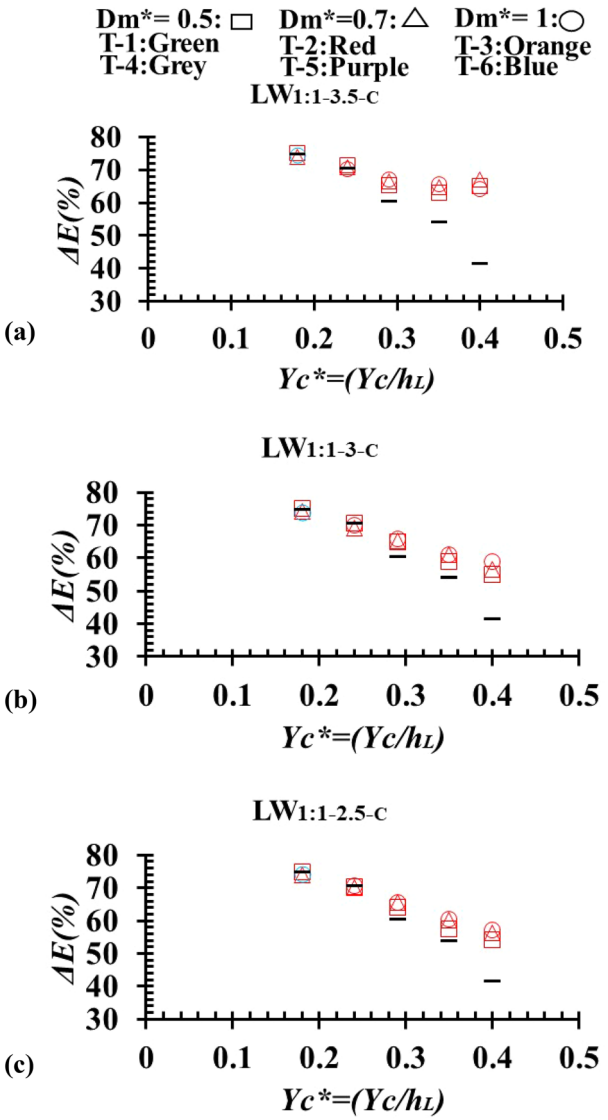

Fig. 11 Energy reduction rate for the cases with landward slope 1:1. **a** Case $LW_{1:1-3.5-C}$, **b** case $LW_{1:1-3-C}$, **c** case $LW_{1:1-2.5-C}$

structure T-2 T-6 was preferable due to maximum energy reduction rate. The results of the present study are valid for the above non-dimensional L_m*, D_m*, Y_c* parameters. The findings could be altered if the levee height is considered twice while keeping all other factors L_m*, D_m*, and Y_c* constant. In the future, further study of the fixed and moveable beds is necessary to achieve flow structures T-2 and T-6 at all overflow water depths. This study did not take into account the evaluation of moat shape by overflowing. The outcomes may be different from the presented one's if the dimensions of the moat are changed with time due to the overflow. A further study is required to investigate the role of the moat by considering other parameters, including the eroded shape of the moat (length and depth of the moat will change with overtopping depth) and other hydraulic parameters. The author would also like to recommend investigating the

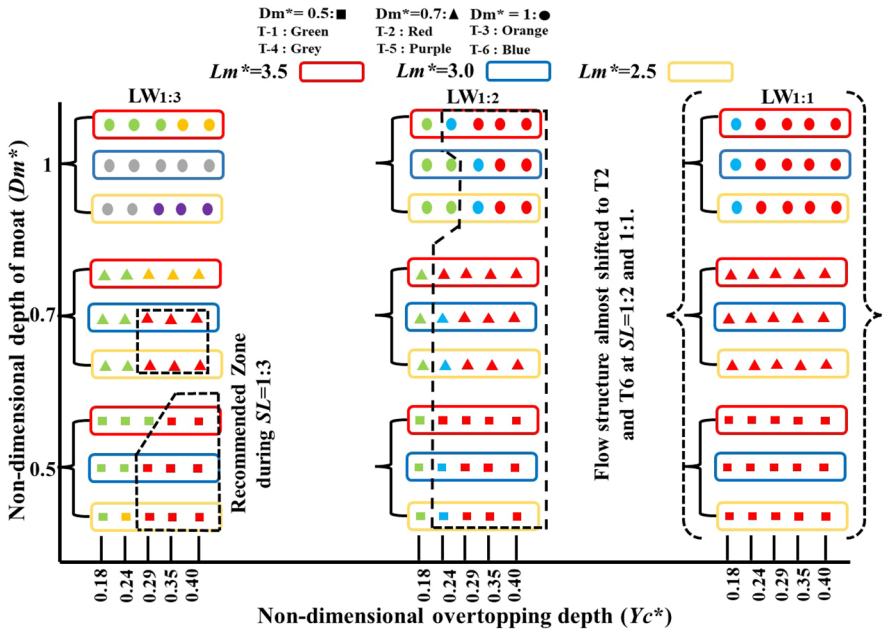

Fig. 12 Flow structure classification and recommended zone to achieve T-2 and T-6

stability of the moat against extreme flow structure, turbulence and variation in flow structures if the moat is eroded.

5 Conclusion

This study proposed the utilization of a water cushion at the toe region of a levee by providing a moat acting as a water cushion to minimize the energy of overflowing flood water. Thirty different cases with 150 experimental trials were conducted to better analyze the variation in the flow regimes and energy reduction rates in LW (levee with moat) cases. As the water cushion body, a moat with changing dimensions of non-dimensional length Lm^* and depth D_m^* was provided on the inland side of a levee having varied landward slopes (S_L). The following outcomes are deduced from the current study.

- The difference in energy reduction between levee with moat (LW) and only levee (OL) systems was minor at the lowest overflow depth (Y_c^*), while the energy reduction rate was approximately 25% larger at higher overflow depth (Y_c^*) in the LW system due to the generation of a hydraulic jump and the counterforce offered by the moat.
- In the LW system, six different flow structures (T-1, T-2, T-3, T-4, T-5, and T-6) were observed after overflowing of the levee. The landward slope (S_L), non-dimensional length of moat (L_m^*), and depth of moat (D_m^*) contributed greatly to the variation in flow structure and hydraulic jump formation. All the flow structures significantly contributed the energy reduction rate, but the maximum energy reduction rate of 25% was

observed during flow structure T-2and T–6, while it was up to 18%, 16%, 17%, and 8% in T-3, T-4, and T-5, and T-1, respectively, as compared to OL case.

- The flow structures T-2 and T-6 were achieved by decreasing non dimensional length (Lm^*) and depth (Dm^*) of moat during landward slope ($S_L = 1{:}3$).Whereas, the flow structure was almost shifted towards T-2 and T-6 by changing landward slope (S_L) 1:3–1:2 and 1:1 respectively.

Although the energy of the overflowing water in flow structures T-1, T-3, T-4, and T-5 was reduced, but T-2 and T-6 may be preferable to sustain the structure due to the presence of submerged hydraulic jump which started from the slope of the levee, covering the whole moat and sufficient increase in water depth inside the moat. The flow structures in this experimental study significantly reduced the energy of the overflowing water from a levee.

The finding of this paper are important for the ideal design procedures of the rectangular moat structure behind the levee system. Furthermore, a constant levee height was used in this research; however, if the levee is raised or lowered, the flow structures and energy reduction behavior would alter. Therefore, further study is needed by considering the varying heights of levee and shapes of the moat along with a moveable bed is necessary to investigate the flow structures, energy reduction, and scouring phenomena behind the LW system.

Declarations

Conflict of interest The authors declare no conflicts of interest for this study.

References

1. Tobita D, Kakinuma T, Yokoyama H, Takeda A (2014) Quantification of leevee breach volume based on levee breach at the Chiyoda experimental flume. J JSCE 2(4):136–143
2. Dewals B, Rifai I, Abderrazek KE, Greco M, Cristo CD, Iervolino M, Leopardi A, Vacca A (2018) Numerical simulation of lateral dike breaching due to overflow. River Flow 03025:1–8
3. Luo P, He B, Takara K, Xiong YE, Nover D, Duan W, Fukushi K (2015) Historical assessment of Chinese and Japanese flood management policies and implications for managing future floods. Environ Sci Policy 48:265–277
4. Tappin DR, Evans HM, Jordan CJ, Richmond B, Sugawara D, Kazuhisa G (2012) Coastal changes in the Sendai area from the impact of the 2011 Tōhoku-oki tsunami: interpretations of time series satellite images, helicopter-borne video footage and field observations. Sediment Geol 282:151–174
5. Tanaka N, Yagisawa J, Yasuda S (2013) Breaking pattern and critical breaking condition of Japanese pine trees on coastal sand dunes in huge tsunami caused by Great East Japan earthquake. Nat Hazards 65(1):423–442
6. Muhammad RAH, Tanaka N (2019) Energy reduction of a tsunami current through a hybrid defense system comprising a sea embankment followed by a coastal forest. Geosciences 9(6):1–27
7. Igarashi Y, Tanaka N, Zaha T (2018) Changes in flow structures and energy reduction through compound tsunami mitigation system with embankment and lined piles. Ocean Eng 164:722–732
8. Tanaka N, Yasuda S, Iimura K, Yagisawa J (2014) Combined effects of coastal forest and sea embankment on reducing the washout region of houses in the Great East Japan tsunami. J Hydro-Environ Res 8(3):270–280
9. Tokida KI, Tanimoto R (2014) Lessons for countermeasures using earth structures against tsunami obtained in the 2011 off the pacific coast of Tohoku earthquake. Soils Found 54(4):523–543
10. Igarashi Y, Tanaka N (2018) Effectiveness of a compound defense system of sea embankment and coastal forest against a tsunami. Ocean Eng 151:246–256

11. Usman F, Murakami K, Kurniawan EB (2014) Study on reducing tsunami inundation energy by the modification of topography based on local wisdom. Procedia Environ Sci 20:642–650
12. Rahman MM, Schaab C, Nakaza E (2017) Experimental and numerical modeling of tsunami mitigation by canals. J Waterw Port Coast Ocean Eng 143(1):1–11
13. Niimi T, Kawasaki K, Mabuchi Y, Nagayama K, Tsuji T, Oie T, Matsuda K (2013) Numerical examination on tsunami mitigation effect of Teizan canal. J JSCE Coast Eng 69(2):211–215
14. Tsujimoto G, Mineura R, Yamada F, Kakinoki T, Uno K (2014) Scouring mechanism behind seawall from tsunami overflow and optimum conditions to reduce tsunami energy with an artificail trench. In: Proceedings of the coastal engineering conference, pp 1–7
15. Mineura R, Tsujimoto G, Yamada F (2013) A study on scouring by overflow from seawall and application of an artificial trench. J JSCE Ser B2 Coast Eng 69:791–795
16. Tanaka N, Igarashi Y (2016) Multiple defense for tsunami inundation by two embankment system and prevention of oscillation by trees on embankment. In: Proceedings of the 20th congress of IAHR APD congress. Colombo, Sri Lanka, pp 28–31
17. Zaha T, Tanaka N, Kimiwada Y (2019) Flume experiments on optimal arrangement of hybrid defense system comprising an embankment, moat, and emergent vegetation to mitigate inundating tsunami current. Ocean Eng 173(11):45–57
18. Correia AS (2017) Tsunami mitigation in Japan after the 2011 Tōhoku tsunami. Int J Disaster Risk Reduct 22:397–411
19. Tanaka N (2009) Vegetation bio shields for tsunami mitigation: review of effectiveness, limitations, construction, and sustainable management. Landsc Ecol Eng 5:71–79
20. Matsuba S, Mikami T, Jayaratne R, Shibayama T, Esteban M (2014) Analysis of tsunami behavior and the effect of coastal forest in reducing tsunami force around coastal dikes. In: Proceedings of the coastal engineering conference
21. Pasha GA, Tanaka N (2017) Undular hydraulic jump formation and energy loss in a flow through emergent vegetation of varying thickness and density. Ocean Eng 141:308–325
22. Tanaka N, Jinadasa KBS, N, Mowjood M I M, Fasly M S M, (2011) Coastal vegetation planting projects for tsunami disaster mitigation: effectiveness evaluation of new establishments. Landsc Ecol Eng 7(1):127–135
23. Mitobe Y, Adityawan MB, Tanaka H, Kawahara T, Kurosawa T, Otushi K (2014) Experiments on local scour behind coastal dikes induced by tsunami overflow. Coast Eng Proc
24. Takegawa N, Sawada Y, Kawabata T (2019) Geogrid-based countermeasures against scour behind coastal dikes under tsunami overflow. Mar Georesour Geotechnol 38(1):64–72
25. Johnson EB, Testik FY, Ravichandran N, Schooler J (2013) Levee scour from overtopping storm waves and scour counter measures. Ocean Eng 72:72–82
26. Rahman MA, Tanaka N, Rehman N (2021) Experimental study on reduction of scouring and tsunami energy through a defense system consisting a seaward embankment followed by vertically double layered vegetation. Ocean Eng 234:108816
27. Rao BR (2005) Buckingham canal saved people in Andhra Pradesh (India) from the tsunami of 26 Dec 2004. Curr Sci 89(1):12–13
28. Tanaka N, Sato M (2015) Scoured depth and length of pools and ditches generated by overflow flow from embankments during the 2011 Great East Japan tsunami. Ocean Eng 109:72–82
29. Kimiwada Y, Tanaka N, Zaha T (2020) Differences in effectiveness of a hybrid tsunami defense system comprising an embankment, moat, and forest in submerged, emergent, or combined conditions. Ocean Eng 208:107457
30. Li LX, Sheng LH, Da L, Sheng-yin J (2015) Experimental investigation of the optimization of stilling basin with shallow-water cushion used for low Froude number energy dissipation. J Hydrodyn 27(4):522–529
31. Li Q, Li L, Liao H (2018) Study on the best depth of stilling basin with shallow-water cushion. Water (Switzerland) 10(12):1–16
32. Tokida K, Tanimoto R (2012) Resistance of earth bank against tsunami and structure of dug pool formed by tsunami in the 2011 off the pacific coast of Tohoku earthquake (in Japanese with english abstract). Japan Sco of Civi Eng 68(4):1091–1112
33. Larsen BE, Arboll LK, Kristoffersen SF, Carstensen S, Fuhrman DR (2018) Experimental study of tsunami-induced scour around a monopile foundation. Coast Eng 138:9–21
34. Rashedunnabi AHM, Tanaka N (2019) Energy reduction of a tsunami current through a hybrid defense system comprising a sea embankment followed by a coastal forest. Geosciences 9:247
35. Ahmed A, Ghumman AR (2019) Experimental investigation of flood energy dissipation by single and hybrid defense system. Water 11:1971

36. Costa DR, Tanaka N (2020) Role of hybrid structures on the control of tsunami induced large driftwood. Coast Eng 163:103798
37. Novak P, Moffat A, Nalluri C, Narayanan R (2014) Hydraulic Structures, 4th edn. CRC Press, Boca Raton, FL, USA
38. Peakall J, Warburton J (1996) Surface tension in small hydraulic river models, the significance of the Weber number. J Hydrol New Zeal 35:199–212
39. Kyuka T, Okabe K, Shimizu Y, Kazuyoshi H, Shinjo K (2020) Dominating factors influencing rapid meander shift and levee breaches caused by a record-breaking flood in the Otofuke river. Japan J Hydro-Environ Res 31:76–89
40. van Bergeijk VM, Warmink JJ, Van Gent MRA, Hulscher SJMH (2019) An analytical model of wave overflow flow velocities on dike crests and landward slopes. Coast Eng 149:28–38
41. Shimozono T, Sato S (2016) Coastal vulnerability analysis during tsunami-induced levee overflow and breaching by a high-resolution flood model. Coast Eng 107:116–126
42. Wei HY, Yu MH, Wang DW, Li YT (2016) Overtopping breaching of river levees constructed with cohesive sediments. Nat Hazard 16(7):541–1551
43. Silva-Araya W F., Alva-Solari L, Chaudhry M H (2010) Experimental study of levee breach.In: 21st century watershed technology: improving water quality and environment, pp 423–429
44. Jayaratn MPR, Premaratne B, Premaratne B, Adewale A, Mikami T, Matsuba S, Shibayama T, Esteban m, Nistor L, (2016) Failure mechanisms and local scour at coastal structures induced by tsunami. Coast Eng J 58(04):1640017
45. Chow V. Te (1959) Open Channel Hydraulics McGraw-Hill, New York 26–27
46. Hager WH (1988) B-jump in sloping channel. J Hydraulic Res. 26(5):539
47. Ohtsu BI, Yasuda Y (1991) Hydraulic jump in sloping channels. J Hydraulic Eng 117:905–921
48. Ali A, Pasha GA, Ghani U, Ahmed A, Abbas F (2019) Investigating role of vegetation in protection of houses during floods. Civil Eng J 5(12):2598–2613
49. Rashedunnabi AHM, Tanaka N (2018) Effectiveness of double-layer rigid vegetation in reducing the velocity and fluid force of a tsunami inundation behind the vegetation. Ocean Eng 201:107142